# *Ab initio* study of electronic and optical properties of multiwall carbon nanotube structures made up of a single rolled-up graphite sheet

Hui Pan, Yuanping Feng,* and Jianyi Lin
*Department of Physics, National University of Singapore, 2 Science Drive 3, Singapore 117542*
(Received 1 February 2005; revised manuscript received 27 April 2005; published 3 August 2005)

The electronic and optical properties of carbon nanoscrolls were investigated using a first-principles method based on density functional theory and the local density approximation (LDA). Two models of different sizes were considered and their properties were compared. The nanoscrolls were found to be metallic and semimetallic within the LDA. The energy bands near the Fermi level were ascribed to the bonding unsaturation at the edges of the carbon nanoscroll. Increasing the size of the nanoscroll resulted in decoupling between the *p* orbitals at the inner and outer edges. The calculated reflection spectra and loss function showed features of both single-wall carbon and multiwall carbon nanotubes.

DOI: 10.1103/PhysRevB.72.085415 PACS number(s): 61.48.+c, 68.43.−h, 73.22.−f, 71.15.Mb

Since its discovery,[1] the carbon nanotube (CNT) has attracted ever increasing scientific interest due to its outstanding mechanical and electronic properties. Experimentally, CNT's can be synthesized by the laser-vaporization method, electric-arc discharge technique, or chemical vapor deposition (CVD).[2,3] Theoretically, a carbon nanotube can be considered as a graphite sheet curled up into a cylinder. Generally, CNT's can be classified into single-wall carbon nanotubes (SWCNT's) (one cylinder of the graphite sheet) and multiwall carbon nanotubes (MWCNT's). Intensive researches have been carried out on both types of nanotubes. The structure of a SWCNT is completely described by a chiral vector $\vec{R}=n\vec{C}_1+m\vec{C}_2$ or simply $(n,m)$, where $\vec{C}_1$ and $\vec{C}_2$ are basis vectors of a graphite plane.[4] The electronic properties of SWCNT's are dependent on their chirality and diameters.[5–10]

MWCNT's can be further divided into two categories: the Russian doll and the Swiss roll (carbon nanoscroll).[11] The Russian doll structure consists of nested carbon tubes, while the Swiss roll structure is made up of a single rolled-up graphite sheet.[1,12–16] Most studies of MWCNT's have been focused on the Russian doll structures. The intershell spacing $d_{002}$ in Russian dolls was found to range from 0.34 to 0.39 nm, increasing with decreasing tube diameter.[17,18] The Swiss roll structure was first thought as defects in CNT's.[13] But its existence was eventually confirmed by x-ray diffraction.[15] Recently, Ruland *et al.* demonstrated that the Swiss roll structure has a uniform chirality.[16] Further studies have been carried out to investigate the structural stability and properties of this new form of carbon.[17,19–22] However, compared to the Russian dolls, the Swiss roll is still a relatively unknown system. Systematic investigations of the structural and electronic properties of this unique nanostructure would be useful for understanding its structure and properties and for exploring its potential applications, such as sensors, hydrogen storage, and nanodevices.

However, a theoretical study of CNT's, particularly MWCNT's or nanoscrolls, is difficult due to the large number of atoms required to model the system. Initial calculations of carbon nanoscrolls were carried out using continuum elasticity theory[19–22] which cannot reveal structural features at the atomic level. Setton carried out a molecular mechanics calculation but used only a pairwise interaction.[23] More recently, Braga *et al.* performed molecular dynamics simulations to investigate the formation, stability, and structural effect of carbon nanoscrolls due to charge injection[24] and found that carbon nanoscrolls automatically occur when a critical overlap between sheet layers is achieved for the partially curled sheet and charge injection causes them to unwind. However, to our knowledge, there has not been any systematic investigation of the electronic properties of such structures, particularly using first-principles methods. With unprecedented accuracy, first-principles calculations can be expected to reveal more details of the structure and properties of the carbon nanoscrolls and provide further understanding of this unique type of nanostructures.

In this study, we investigate the electronic and optical properties of carbon nanoscrolls using a first-principles method based on density functional theory (DFT) and the local density approximation (LDA). The plane-wave basis DFT pseudopotential method[25] and the CASTEP (Cambridge serial total energy package) code[26] were used in our study. In the total energy calculations, the ionic potentials were described by an ultrasoft nonlocal pseudopotential proposed by Vanderbilt.[27] The exchange-correlation function parametrized by Perdew and Zunger was used.[28] We used a supercell of $25\times25\times2.438$ Å$^3$ which is sufficient to avoid an interaction of the nanoscroll with its images. An energy cut off of 310 eV was used for the plane-wave expansion of the electronic wave function. Ten *k* points along the direction of the tube axis were chosen according to the Monkhorst-Pack scheme for the sampling of *k* points in the Brillouin zone.[29] Good convergence was obtained with these parameters. The total energy was converged to $2.0\times10^{-5}$ eV/atom while the Hellman-Feynman force was smaller than $5.0\times10^{-2}$ eV/Å in the optimized structure.

Nanoscrolls with chirality equivalent to that of the armchair carbon nanotube were chosen in our study, for convenience of modeling. That is, the carbon nanoscrolls were obtained by rolling up a graphite sheet in the direction of $\vec{R}_n=n\vec{C}_1+n\vec{C}_2$. In order to investigate the size dependence of the electronic and optical properties of the nanoscroll, calcu-

 

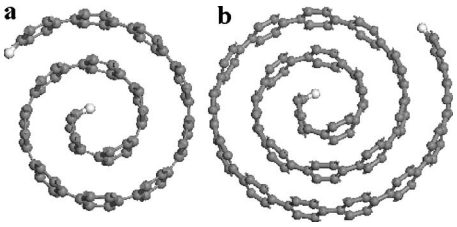


FIG. 1. Initial structures of (a) Model 1 and (b) Model 2 of carbon nanoscrolls. Carbon and hydrogen atoms are shown in black and white balls, respectively.

lations were performed on two models which differ only in their sizes. Model 1, shown in Fig. 1(a), has $n=14$ while model 2, shown in Fig. 1(b), corresponds to $n=24$. Dangling bonds at the edges of the graphite sheet were saturated using hydrogen atoms which are shown using white balls in Figs. 1 and 2. Hydrogenation of edge carbon atoms is physically possible due to the presence of hydrogen atoms in the growth process. The carbon nanoscrolls were constructed from a structurally optimized graphite sheet in which the C—C bond length is 1.41 Å and the distance between two adjacent graphite layers is 3.41 Å. The bond length is close to the experimental value of 1.42 Å. The atomic structures of the carbon nanoscrolls were then fully optimized through minimization of their total energies by means of the Hellman-Feynman forces, including Pulay-like corrections.[30]

Figure 2 shows the atomic structures of the two models after geometry optimization. Compared to the initial structures shown in Fig. 1, it is clear that the inner half-circle of the graphite sheet extends after the optimization, to relax the strain. At the same time, the outer part of the nanoscroll extends outward slightly. The interlayer spacing is about 3.42 Å, which is similar to that of graphite or the Russia doll, except near the edges of the graphitic sheet. The interlayer distance is smaller (3.13 Å) near the inner edge, while it is larger near the open end (3.45 Å for model 1 and 3.55 Å for model 2) due to the extension of the graphitic sheet. It is interesting to note that the structure of model 1 is very similar to the equivalent section of model 2. The C—C bond length is constant (1.42 Å) except near the edges, where the bond extends to 1.43 Å near the inner edge and 1.44 Å near the open edge. The bond angles are also uniform ($\sim 119°$) except near the edges, where the bond angle expands to about 122° and there is essentially no difference between the inner edge and the open edge. The changes in bond lengths and bond angles near the free ends can be expected. Other

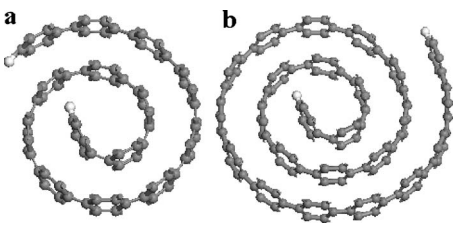


FIG. 2. Optimized structures of (a) Model 1 and (2) Model 2 of carbon nanoscrolls. Carbon and hydrogen atoms are shown in black and white balls, respectively.

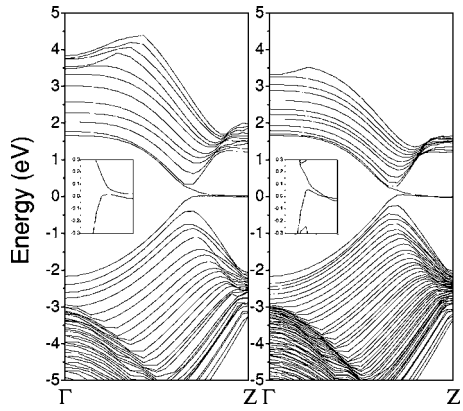


FIG. 3. Calculated band structures of (a) Model 1 and (b) Model 2 of the carbon nanoscrolls. The insets are the fine structures of the valence band top and conduction band bottom. The Fermi level is indicated by the dashed line.

than that, the structural properties of the nanoscroll are similar to those of SWCNT's and the Russia doll, and there is essentially no difference in interlayer spacing, bond lengths, and bond angles between these structures. This is reasonable because the interlayer couplings in all these structures are weak and the properties of these structures are mainly determined by their chirality and curvature. Results of our calculation are consistent with the experimental results.[16] However, it should be pointed out that even though our structural optimization has converged, whether carbon nanoscrolls of such small sizes can be stable remains to be investigated. In the following, we focus on the electronic and optical properties of the carbon nanoscrolls.

The symmetry of an achiral carbon nanotube, armchair $(n,n)$ or zigzag $(n,0)$, is expressed by a direct group product $D_n \otimes C_i$,[4] which depends on whether $n$ is even or odd. When $n$ is even, the product is $D_{nh}$; otherwise, it is $D_{nd}$. It is known that all armchair nanotubes are metallic with two bands crossing the Fermi level at $k=\pm 2\pi/(3a)$, where $a=2.47$ Å is the lattice constant of graphite. These two bands are nondegenerate and form the $\pi$ and $\pi^*$ states. Most of other energy levels are doubly degenerate. The symmetry of the nanoscroll is lower than that of the armchair nanotube, and it belongs to the point group of $C_s$. The $\pi$ state is thus distorted, which results in a split of the degenerate states. Figure 3 shows the calculated band structures of the two models. All energy levels of the scroll structure are nondegenerate, due to the lower symmetry, in contrast to those of the tube structure. The overall band structures of the two models are similar. Compared to the band structure of a single-wall armchair carbon nanotube,[31] the two bands that cross each other now split, due to interlayer interaction. This is similar to that in a double-wall carbon nanotube where the same two bands split due to the intertube interaction and result in an opening of pseudo energy gaps.[18] However, these two bands in the nanoscrolls remain close to each other near the Brillouin-zone boundary. By considering scrolled carbon as a curled graphite sheet these two energy levels may result from the bonding unsaturation at the edges of the graphene sheet. They may be denoted as the conduction-band edge state (CES for the one above the Fermi level) and valence-band

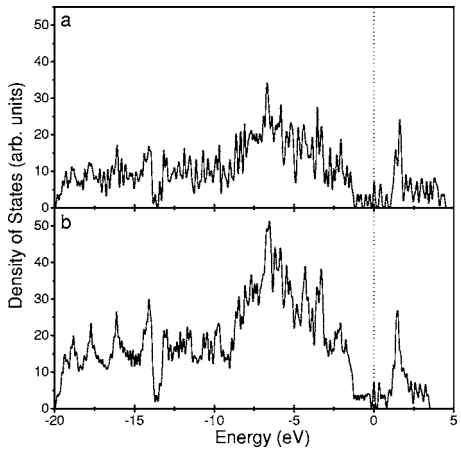


FIG. 4. Calculated total density of states for (a) Model 1 and (b) Model 2, respectively. The Fermi level is indicated by the dashed line.

edge state (VES for the one below the Fermi level). It is interesting to note that the CES level and the VES level of model 1 come very close to each other but do not intersect, as shown in the inset of Fig. 3(a), indicating that the carbon nanoscroll is a semimetal. But for model 2, the same two energy levels cross each other, as shown in the inset of Fig. 3(b). The larger carbon nanoscroll appears to be metallic within the LDA. Figure 4 shows the total density of states (TDOS) of the two models. The peak around −6.0 eV in the TDOS of model 1 [Fig. 4(a)] is mainly due to the $pp\sigma$ bonds because the $pp\sigma$ states are unaffected by the change of symmetry and dominate the bonding in the scroll. A small peak in the TDOS can be seen around the Fermi level, which is induced by the valence-band edge state, as shown in Fig. 3(a). The general features of the TDOS of model 2 [Fig. 4(b)] are the same as those of model 1.

Figure 5 shows the electron densities of the valence-band edge state and conduction-band edge state of both models. The electron densities have been summed over all $k$ points in the Brillouin zone. For model 1, the VES and CES are mainly contributed by the $p$ orbitals of the carbon atoms near

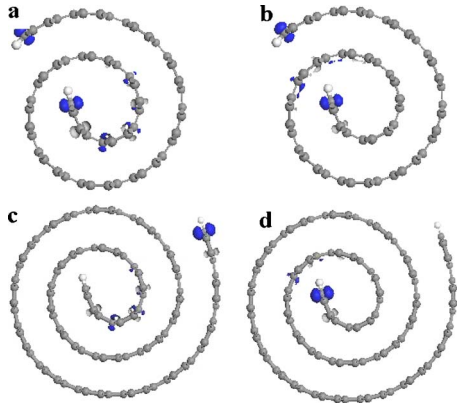


FIG. 5. (Color online) The electron density of (a) the valence band edge state of Model 1; (b) the conduction band edge state of Model 1; (c) the valence band edge state of Model 2; and (d) the conduction band edge state of Model 2.

the inner and outer edges. These $p$ orbitals are perpendicular to the axis of the scroll and contribute to the formation of the $\pi$ state in the SWCNT's (tube $\pi$ state). In the scroll structure, the $p$ orbitals of the carbon atoms near the edges separate from the tube $\pi$ state and form $\pi$ states (edge $\pi$ states) along the scroll axis near the edges of the graphite sheet. The separation of the edge $\pi$ states from the tube $\pi$ states could be due to the curvature effect. That is, different curvatures near the edges of the graphite sheet and that in the rest of the nanoscroll result in the splitting of the $\pi$ state normally observed in SWCNT. For model 2, the electron densities of the same orbitals [Figs. 5(c) and 5(d)] show that the VES has its origin from the $p$ orbital of the carbon atom at the open end of the nanoscroll [Fig. 5(c)], while the CES results mainly from the $p$ orbitals of the carbon atoms near the inner end of the graphite sheet [Fig. 5(d)], which is different from model 1. Comparing the charge densities corresponding to the VES and CES of the two models given in Fig. 5, we can see that $p$ orbitals from carbon atoms near both ends of the nanoscroll in model 1 contribute to these energy levels. However, in model 2, the $p$ orbital of the carbon atoms near the open end is mostly filled with electrons while that near the inner end is largely unoccupied. Thus, increasing the size of the nanoscroll results in decoupling between the $p$ orbitals at the two ends. It can be concluded that the curvature effect of the inner part pushes the CES up and separates the VES and CES, as in model 1, but this effect diminishes with increase in the size of the nanoscroll.

Compared to SWCNT's and MWCNT's, nanoscrolls show certain unique electronic properties. First of all, nondegenerate states dominate in nanoscrolls, in contrast to the doubly degenerate states in SWCNT's. Furthermore, for the small nanoscroll (model 1), the VES and CES are very close but remain on separate sides of the Fermi level, $E_F$, resulting in a pseudogap. It was reported that a gap or a pseudogap can be induced in MWCNT's composed of metallic armchair tubes due to intertube interaction or reduced symmetry.[18] Similarly, the pseudogap observed here in model 1 can be attributed to the reduced symmetry and the curvature effect of the nanoscroll. The pseudogap disappears as the number of overlapping layers increases, as observed in model 2. It is noted that the electronic properties of the nanoscroll are related to the number of overlapping layers in the scroll. The metallic property of the tube is restored when the number of overlapping layers reaches a certain value.

Theoretical studies on optical properties of SWCNT's and MWCNT's have been reported.[32–35] A special structure at $\omega \sim 2\gamma_0$, where $\gamma_0(\sim 2.4-3.0$ eV) is the nearest-neighbor overlap integral,[6] has been observed for MWCNT's.[34] We calculated, and in the following give a comparison of, the reflection spectra and loss functions of the two models.

The reflectance spectra were calculated for a periodic system from $R(\omega)=|1-\sqrt{\varepsilon(\omega)}|^2/|1+\sqrt{\varepsilon(\omega)}|^2$, where $\varepsilon(\omega)=\varepsilon_1(\omega)+i\varepsilon_2(\omega)$ is the macroscopic dielectric function. Figures 6(a) and 6(b) show the calculated reflectance spectra ($R$) for light polarization perpendicular and parallel to the axis of the nanoscroll, respectively. In the case of perpendicular light polarization, $R$ decreases first, reaches a minimum, and then increases, as $\omega$ increases from zero to $\omega_0(\sim 1.1$ eV). The

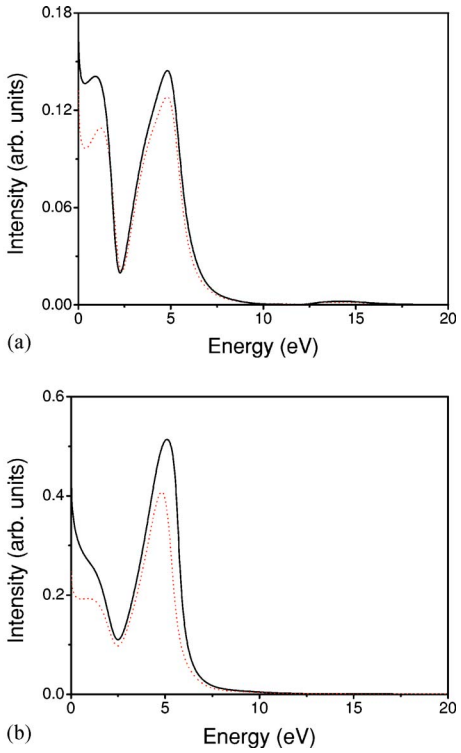


FIG. 6. (Color online) Reflection spectra of the two models, (a) for light polarization perpendicular to the nanoscroll's axis; (b) for light polarization parallel to the nanoscroll's axis. The dashed line (solid line) is for Model 1 (Model 2).

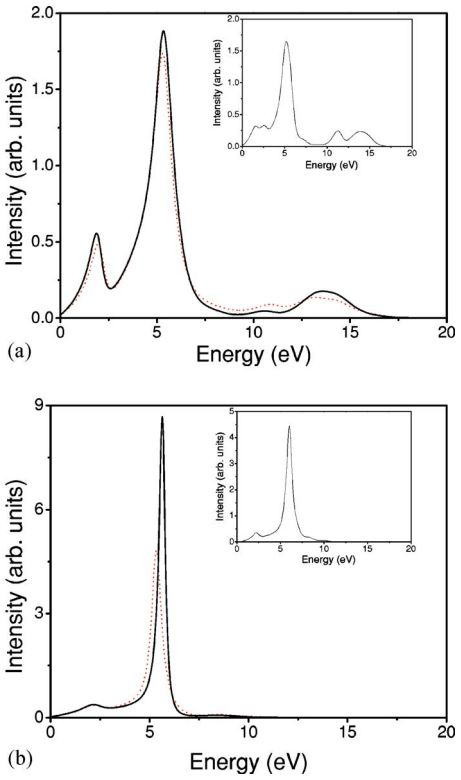


FIG. 7. (Color online) Loss functions of the two models, (a) for light polarization perpendicular to the nanoscroll's axis; (b) for light polarization parallel to the nanoscroll's axis. The dashed line (solid line) is for Model 1 (Model 2). The insets show loss functions of the armchair carbon nanotube (10, 10).

reflectance spectrum reaches a peak at $\omega=\omega_0$. Beyond the peak, $R$ decreases rapidly as a function of $\omega$, reaches the second minimum, and then increases rapidly again, until reaching the second peak at $2\gamma_0$ ($\sim$4.9 eV in our calculation). With a further increase in $\omega$, $R$ drops to 0 rapidly. The small peak at $\omega_0$ is not apparent under the parallel light polarization, particularly for model 2, as shown in Fig. 6(b). Generally, the frequency-dependent reflectance spectrum of the nanoscroll is similar to that of MWCNT's,[34] except the peak at $\omega_0$. For example, the peak at $\omega=2\gamma_0$ and an abrupt $\pi$-plasmon edge at $\omega>2\gamma_0$ are typical features of reflectance spectra of MWCNT's. However, the peak at $\omega_0$ is only observed in SWCNT's,[36] and its position is upshifted with an increase in the diameter of the SWCNT's. This low-frequency peak corresponds to the transition between DOS peaks of the tubes. In this aspect, the optical properties of carbon nanoscrolls are similar to those of the corresponding SWCNT's. Comparing the reflectance spectra of the two models, no major difference is observed, except the intensity of the spectrum, especially at $\omega_0$.

The loss functions, calculated from $\mathrm{Im}[-1/\varepsilon(\omega)]$ at zero-momentum transfer, are shown in Figs. 7(a) and 7(b), for light polarization perpendicular and parallel to the axis of the scroll, respectively. Several peaks, including a pronounced one near $2\gamma_0$, can be seen in the loss functions of both nanoscrolls. The pronounced peak at $\omega=2\gamma_0$ can be attributed to the collective excitations of $\pi$ electrons. The $\pi$ plasmon is weaker for the perpendicular polarization than that for the parallel polarization, due to the fact that optical excitation is less effective in the perpendicular case. Under perpendicular light polarization, peaks are also observed in the high-frequency region ($\omega\sim$13.5 eV). These peaks are attributed to the high-frequency $\pi+\sigma$ plasmon.[33] There exists another peak around $\omega\sim$2.0 eV in the loss function of the nanoscroll, which is related to the inter-$\pi$-band excitation.[37] This low-frequency excitation, apparent in both polarization conditions, is also seen in the spectra of SWCNT's, but normally does not appear in the spectra of MWCNT's, except those consisting of a very few walls under perpendicular polarization.[36,38] In the latter, the strength of inter-$\pi$-band excitation reduces with the increase in the number of walls.[38]

It is clear in Figs. 7(a) and 7(b), particularly in the case of parallel light polarization, that the strength of the $\pi$ plasmon increases and its peak position upshifts with the increase of overlapping layers in the nanoscrolls which results from the increased number of carbon atoms and thus enhanced strength of the $p$ orbitals. This is similar to the size effects in MWCNT's where the $\pi$ plasma was also enhanced and upshifts with the increase in number of walls.[38] On the other hand, the inter-$\pi$-band excitation is also strengthened but the peak position slightly downshifts as the overlapping layers increase. This is because the spacing between energy levels decreases with an increasing number of atoms due to the splitting of degenerate levels. The downward shift of the inter-$\pi$-band excitation peak is different from that in MWCNT's,[38] but similar to the size effect in SWCNT's

where the inter-$\pi$-band excitation is enhanced and downshifted with the increase in tube diameter.[35] Therefore, the loss function of nanoscrolls behaves like MWCNT's except at the low-frequency region where it is similar to that of SWCNT's.

In summary, we performed first-principles calculations of the electronic and optical properties of carbon nanoscrolls. Our results show that the electronic and optical properties of carbon nanoscrolls are different from those of nanotubes. The electronic properties of the scroll are closely related to the overlapping layers in the scroll. For the small scroll (model 1), the valence-band edge state and the conduction-band edge state are very close but do not cross each other. But for the large scroll (model 2), they are tangled near the Fermi level. The nanoscrolls were found to be metallic and semimetallic within the LDA. Anisotropic properties were observed in the calculated optical properties of the nanoscrolls. Analysis of the reflection and loss function showed that the nanoscroll structure shares properties with both SWCNT's and MWCNT's.

*Corresponding author. Electronic address: phyfyp@nus.edu.sg

[1] S. Iijima, Nature (London) **354**, 56 (1991).
[2] A. Thess, R. Lee, P. Nikolaev, H. Dai, P. Petit, J. Robert, C. Xu, Y. H. Lee, S. G. Kim, A. G. Rinzler, D. T. Colbert, G. E. Scuseria, D. Tománek, J. E. Fischer, and R. E. Smalley, Science **273**, 483 (1996).
[3] T. Guo, P. Nikolaev, A. Thess, D. T. Colbert, and R. E. Smalley, Chem. Phys. Lett. **243**, 49 (1995).
[4] M. S. Dresselhaus, G. Dresslhaus, and P. C. Eklund, *Science of Fullerenes and Carbon Nanotubes* (Acadamic Press, San Diego, 1996).
[5] N. Hamada, S. I. Sawada, and A. Oshiyama, Phys. Rev. Lett. **68**, 1579 (1992).
[6] J. W. Mintmire, B. I. Dunlap, and C. T. White, Phys. Rev. Lett. **68**, 631 (1992).
[7] A. Kleiner and S. Eggert, Phys. Rev. B **63**, 073408 (2001).
[8] J. W. Mintmire and C. T. White, Phys. Rev. Lett. **81**, 2506 (1998).
[9] O. Gulseren, T. Yildirim, and S. Ciraci, Phys. Rev. B **65**, 153405 (2002).
[10] D.-H. Oh and Y. H. Lee, Phys. Rev. B **58**, 7407 (1998).
[11] Peter J. F. Harris, *Carbon Nanotubes and Related Structures: New materials for the 21st century* (Cambridge University Press, New York, 1999).
[12] S. Amelinckx, D. Bernaerts, X. B. Zhang, G. V. Tendeloo, and J. V. Landuyt, Science **267**, 1334 (1995).
[13] O. Zhou, R. M. Fleming, D. W. Murphy, C. H. Chen, R. C. Haddon, A. P. Ramirez, and S. H. Glarum, Science **263**, 1744 (1994).
[14] M. Liu and J. M. Cowley, Carbon **32**, 393 (1994).
[15] G. Xu, Z. Feng, Z. Popovic, J. Lin, and J. J. Vittal, Adv. Mater. (Weinheim, Ger.) **13**, 264 (2001).
[16] W. Ruland, A. K. Schaper, H. Hou, and A. Greiner, Carbon **41**, 423 (2003).
[17] C.-H. Kiang, M. Endo, P. M. Ajayan, G. Dresselhaus, and M. S. Dresselhaus, Phys. Rev. Lett. **81**, 1869 (1998).
[18] Y.-K Kwon and D. Tomanek, Phys. Rev. B **58**, R16001 (1998).
[19] J. G. Lavin, S. Subramoney, R. S. Ruoff, S. Berber, and D. Tomanek, Carbon **40**, 1123 (2002).
[20] D. Tomanek, W. Zhong, and E. Krastev, Phys. Rev. B **48**, 15461 (1993).
[21] D. Tomanek, Physica B **323**, 86 (2002).
[22] M. Grundmann, Appl. Phys. Lett. **83**, 2444 (2003).
[23] R. Setton, Carbon **34**, 69 (1996).
[24] S. F. Braga, V. R. Coluci, S. B. Legoas, R. Giro, D. S. Galvao, and R. H. Baughman, Nano Lett. **4**, 881 (2004).
[25] M. C. Payne *et al.*, Rev. Mod. Phys. **64**, 1045 (1992).
[26] V. Milman, B. Winkler, J. A. White, C. J. Pickard, M. C. Payne, E. V. Akhmatskaya, and R. H. Nobes, Int. J. Quantum Chem. **77**, 895 (2000).
[27] D. Vanderbilt, Phys. Rev. B **41**, 7892 (1990).
[28] J. P. Perdew and A. Zunger, Phys. Rev. B **23**, 5048 (1981).
[29] H. J. Monkhorst and J. Pack, Phys. Rev. B **13**, 5188 (1976).
[30] P. Ordejon, E. Artacho, and J. M. Soler, Phys. Rev. B **53**, R10441 (1996).
[31] S. Reich, C. Thomsen, and P. Ordejon, Phys. Rev. B **65**, 155411 (2002).
[32] F. J. García-Vidal, J. M. Pitarke, and J. B. Pendry, Phys. Rev. Lett. **78**, 4289 (1997).
[33] A. G. Marinopoulos, L. Reining, A. Rubio, and N. Vast, Phys. Rev. Lett. **91**, 046402 (2003).
[34] M. F. Lin, F. L. Shyu, and R. B. Chen, Phys. Rev. B **61**, 14114 (2000).
[35] M. F. Lin, Phys. Rev. B **62**, 13153 (2000).
[36] J. Hwang, H. H. Gommans, A. Ugawa, H. Tashiro, R. Haggenmueller, K. I. Winey, J. E. Fischer, D. B. Tanner, and A. G. Rinzler, Phys. Rev. B **62**, R13310 (2000).
[37] T. Pichler, M. Knupfer, M. S. Golden, J. Fink, A. Rinzler, and R. E. Smalley, Phys. Rev. Lett. **80**, 4729 (1998).
[38] F. L. Shyu and M. F. Lin, Phys. Rev. B **62**, 8508 (2000).